



Article

Hydrothermal Chromitites from the Oman Ophiolite: The Role of Water in Chromitite Genesis

Shoji Arai ^{1,*}, Makoto Miura ², Akihiro Tamura ¹, Norikatsu Akizawa ³ and Akira Ishikawa ⁴¹ Department of Earth Sciences, Kanazawa University, Kanazawa 920-1192, Japan; aking826@gmail.com² Identification Department, GIA Tokyo Godo Kaisha, Yamaguchi Building 7, 4-19-9 Taito, Taito-ku, Tokyo 110-0016, Japan; makomiu1214@gmail.com³ Department of Ocean Floor Geoscience, Atmosphere and Ocean Research Institute, The University of Tokyo, 5-1-5 Kashiwanoha, Kashiwa, Chiba 277-8564, Japan; akizawa@aori.u-tokyo.jp⁴ Department of Earth and Planetary Sciences, Tokyo Institute of Technology, 2-12-1 Ookayama, Meguro, Tokyo 152-8550, Japan; akr@eps.sci.titech.ac.jp

* Correspondence: ultrasa@staff.kanazawa-u.ac.jp

Received: 10 February 2020; Accepted: 26 February 2020; Published: 28 February 2020



Abstract: The role of water-rich solutions in the formation of chromitites has been the matter of controversy. We found small chromite concentrations (chromitites) in diopsidites, precipitated from high-temperature hydrothermal fluids, in the mantle to the crust of the Oman ophiolite. Here, we present petrologic characteristics of the hydrothermal chromitites to understand their genesis. In the chromitites, the chromite is associated with uvarovite in the crust and diopside + grossular in the mantle. They are discriminated from the magmatic podiform chromitite by dominance of the Ca-Al silicates in the matrix. The fluids responsible for chromite precipitation are possibly saline, being derived from the seawater circulated into the mantle through the crust. The saline fluids precipitate chromite to form chromite upon decompression and cooling, and transport platinum-group elements (especially Pt and Pd). The fluids obtain Ca and Al from the crustal rocks and Cr from the mantle rocks during circulation. Saline fluids are also supplied from the slab to the mantle wedge, and can metasomatically precipitate chromite and pyroxenes within peridotites. They re-distribute Cr and chromite in peridotites along with circulation of saline fluids in the mantle wedge.

Keywords: hydrothermal chromitites; Ca-Al silicates; seawater; Oman ophiolite; slab-derived fluids; platinum-group elements

1. Introduction

Chromian spinel or chromite has been recognized as a typical high-T (temperature) igneous mineral, precipitating at an early stage from fractionating magmas or residing in refractory peridotites after magma extraction on partial melting at the mantle [1]. Chromitites, concentrates of chromite or chromian spinel, are therefore considered as plutonic rocks formed from high-T magmas in the upper mantle or within the lower crust [2]. The chromitite in the upper mantle typically occurs as pod-like or irregular forms with a dunite envelope within the mantle peridotite, especially harzburgite [3,4], and are grouped as podiform chromitites. The chromitite in the lower crust typically occurs as layers or seams with ultramafic or anorthositic rocks in layered intrusions, mainly of Precambrian age [5–7], and are grouped as stratiform chromitites.

The stratiform chromitite is formed by crystal accumulation from magmas that filled crustal magma chamber [5,6]. As for the podiform chromitite formation, an igneous origin during a harzburgite-magma reaction in the mantle has been proposed and appears widely accepted [4,8]. The essential role of aqueous solutions in the formation of podiform chromitites in the mantle and other chromitites has

been the subject of controversy [4], and the essential involvement of water in chromitite formation has been proposed [9–15]. Selective severe alteration (serpentinization or metamorphism) in and around chromitite [16,17] reminded early geologists of an essential role of aqueous fluids in formation of chromitite and associated dunite [18–20]. The common presence of Na- and H₂O-rich poly-mineralic inclusions in chromite of chromitites also suggests an essential involvement of H₂O-rich fluid or magma in the podiform chromitite formation [9,10]. The origin of H₂O-rich fluids/magmas for the chromite-hosted inclusion formation has been left unclear and, consequently, their role in chromite concentration has been also left unsettled [4]. Arai and Akizawa [21] and Akizawa and Arai [22] reported occurrences of the chromite clearly precipitated from hydrothermal solutions in the northern Oman ophiolite. The chromite occurs in diopsidites, mainly composed of diopside precipitated from high-T silicate-rich aqueous fluids [23], both in the uppermost mantle and in the lowermost crust exposed in Wadi Fizh of the northern Oman ophiolite [21,22,24,25]. The mantle diopsidite contains thin segregations or pods of chromitite up to several centimeters in thickness [21,22], and the crustal diopsidite encloses micro-pods, less than 1 cm across, of chromitite [21]. Those two chromitites are of clearly hydrothermal origin that has never been described before, although many works have dealt with hydrothermally altered or metamorphosed chromitites of primary igneous origin [17,26,27]. We would like to describe these really hydrothermal chromitites to clarify the petrological and geochemical characteristics of the chromitite formed from hydrothermal fluids. Preliminary discussion was made by Arai and Miura [4].

2. Geologic and Petrographic Background

The northern Oman ophiolite has been famous for its excellent exposure of almost perfect ophiolite stratigraphy from volcanic rocks to metamorphic sole downsection [28]. Deep-seated rocks from the lower crust to the mantle are especially well exposed along Wadi Fizh [29], where we found the hydrothermal chromitites examined in this article (Figure 1).

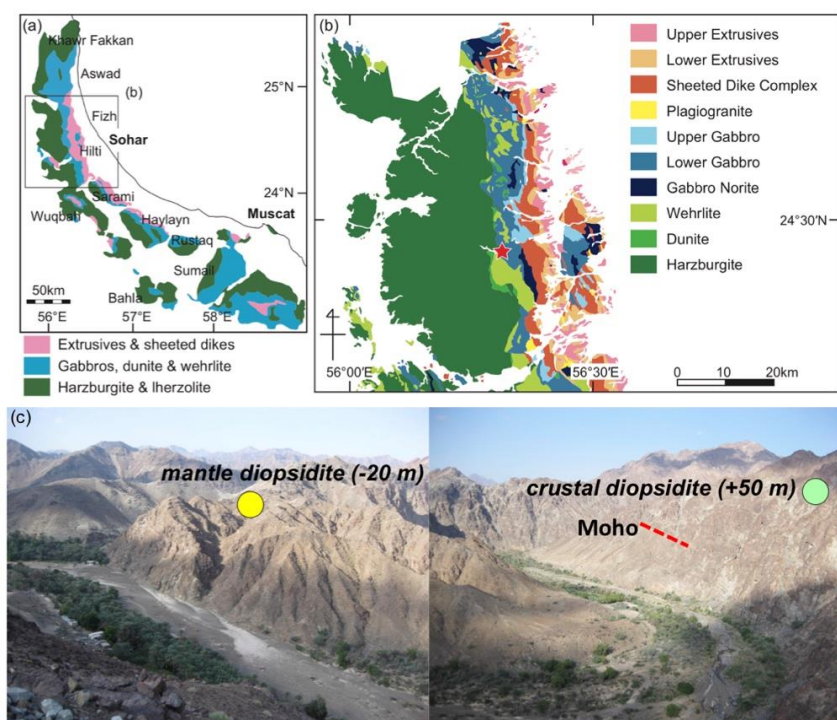


Figure 1. Geological sketch of Fizzh block in the northern Oman ophiolite (a,b) modified and compiled from previous work [28,30,31], and a panoramic view of the uppermost mantle to lower crustal section across Moho along Wadi Fizh (c). The location is represented by star on the geological map. The two diopsidites are about 70 m apart in stratigraphical level across Moho (red broken line).

The Wadi Fizh area is located around a boundary of segments of a spreading ridge responsible for the Oman ophiolite formation, where the Moho transition zone (MTZ) is very thin (~10 m) [29,32], i.e., a lowermost gabbro-dominant portion quickly grades to the harzburgite-dominant mantle section via the dunite-dominant MTZ. The uppermost part (~2 m in thickness) of the MTZ is composed of wehrlite with gabbroic bands and their network [29,32]. We tentatively call the base of the gabbro-dominant portion Moho after Reference [29] in this article. The gabbroic layers just above the Moho have wehrlitic screen, which sharply decreases in amount upward in the lowermost crust (gabbro) section [29,32]. Gabbroic bands decrease in frequency downward in the MTZ to the harzburgite section. They are parallel with the layering of the crustal gabbros and the foliation of the mantle harzburgite (N70°N, 40°E on average [29]). Details of petrologic and geochemical characteristics of the deep-seated rocks around the Moho in this area are described and discussed in detail by Reference [29,33,34].

The crustal diopsidite is located in the layered gabbros located around 20 m above the Moho [24] (Figure 1). The diopsidite gradually changes to surrounding gabbro, which is mainly composed of augitic clinopyroxene and plagioclase (Figure 2a,b). The transitional rock is composed of gabbroic relics in fine-grained aggregates of anorthite and diopside [24]. The diopsidite contains anorthite-rich part (anorthosite). The diopsidite is composed of mainly diopside and anorthite, with a subordinate amount of uvarovite. Minor minerals are chlorite, tremolite, pumpellyite, epidote, and titanite. Minute aqueous fluid inclusions with daughter minerals (calcite or anhydrite) were found in titanite and anorthite [25]. Chromite forms small black clots within the uvarovite-rich part of the diopsidite (Figure 3a).

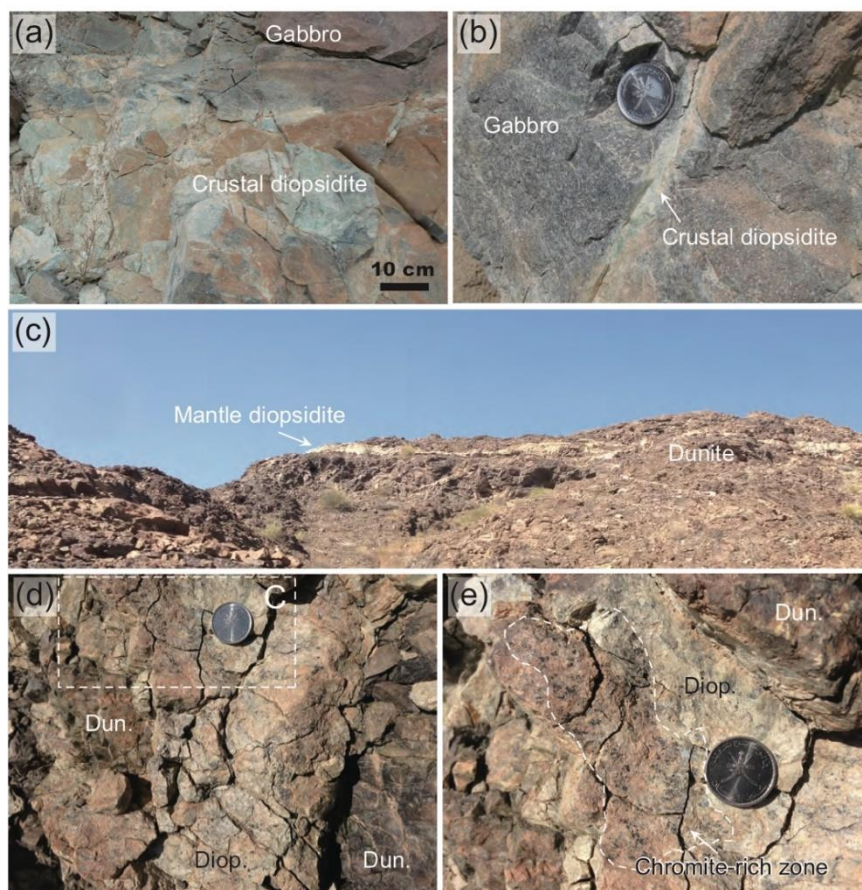


Figure 2. Field photographs of the diopsidites. The coin for scale is 2.3 cm across. (a) Crustal diopsidite replacing layered gabbro. Whitish and greenish parts are anorthite-rich and uvarovite-rich, respectively. (b) Thin diopsidite dike cutting the layered gabbro. (c) Whole view of the mantle diopsidite dikes within dunite. (d) Mantle diopsidite (Diop) in dunite (Dun). (e) Chromite-rich zone of the mantle diopsidite.

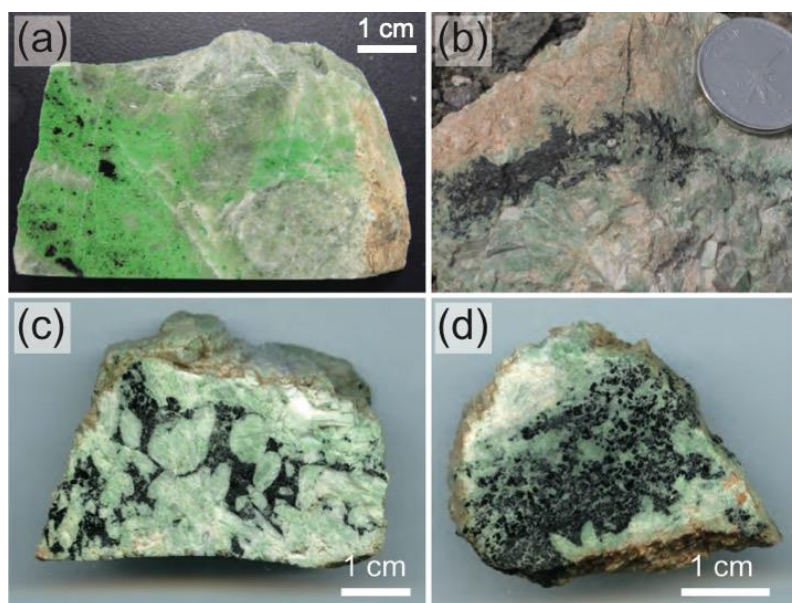


Figure 3. Hand specimen photographs of hydrothermal chromitites. (a) Chromite clots (black) in the crustal diopsidite rich in uvarovite (green). (b) Segregation-like chromitite band in the mantle diopsidite (white to pale green). Chromite fills the interstice of euhedral diopsides. Note a thin veinlet of chromitite branching from the main segregations. The coin is 2.3 cm across. (c) Chromitite as an interstitial aggregate in coarse-grained part of the mantle diopsidite. (d) Chromite-grossular aggregate in part interstitial to coarse diopsidite (green) in the mantle diopsidite.

The mantle diopsidite is located in a harzburgite-dunite portion in the mantle section around 50 m stratigraphically below the Moho [22,25] (Figure 1). It forms a flattened network almost parallel with the gabbro-peridotite boundary upsection [29,33] within the mantle peridotite (Figure 2c). The thickest part reaches 80 cm and has a whitish aureole composed of tremolite [21,22]. The mantle diopsidite is mainly composed of diopside with subordinate grossular instead of uvarovite. The diopside is varied in color from white to pale green, and contains black chromite dots within the greenish part (Figures 2 and 3). Chromite is concentrated as small pod-like to thin segregation-like bodies, less than several centimeters in thickness, in diopsidite, with ragged boundaries with the wall diopsidite [21] (Figures 2 and 3). We recognized a thin chromitite veinlet branching from the main segregations at a high angle (Figure 3b).

3. Petrography of Chromitites (Chromite Concentrations)

The chromite clots (chromitite mini-pods) in the crustal diopsidite (Figure 3a) are fine-grained, mainly composed of chromite, uvarovite, anorthite, and chlorite [21,25] (Figure 4a,b). The minerals are mostly less than 100 microns across. The chromite is euhedral to anhedral and opaque in thin section. It shows optical homogeneity by reflected light under the microscope (Figure 4b). Some euhedral grains are skeletal at their marginal part, where chlorite is closely associated (Figure 4a,b). Chlorite was also observed as minute rounded inclusions in chromite (Figure 4b). The chromites in the small chromite aggregates (Figure 3a) are similar in appearance to disseminated ones in diopsidite reported by Arai and Akizawa [21]. No PGM (platinum-group minerals) have been found under the microscope.

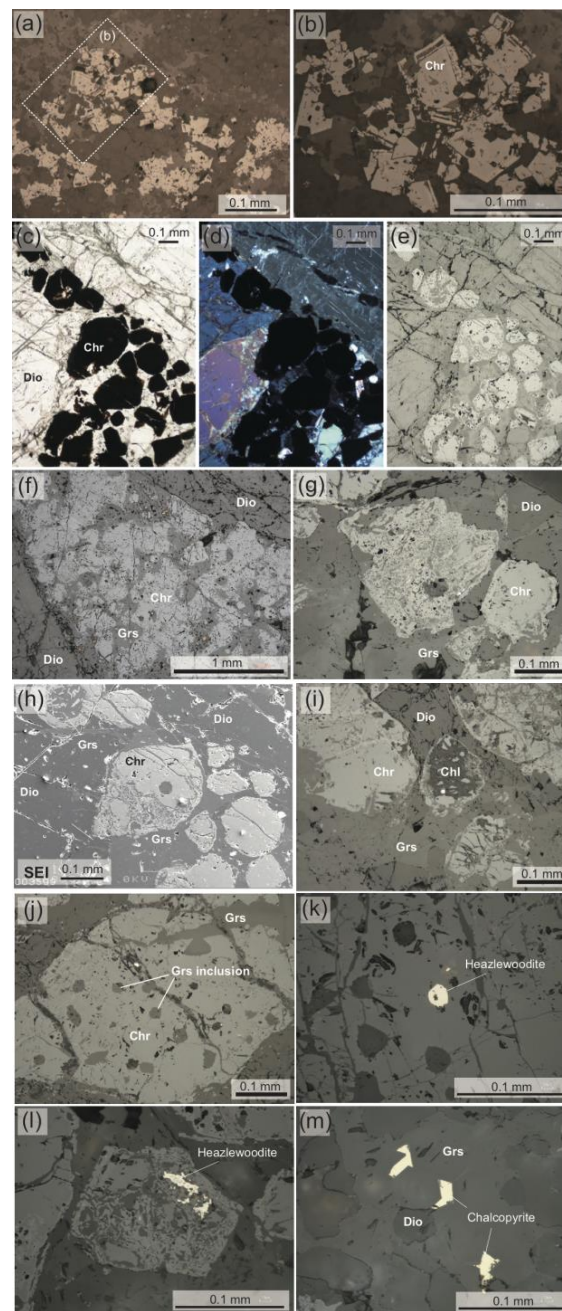


Figure 4. Microscopic textures of the hydrothermal chromitites. (a,b) Chromitite in the crustal diopsidite. (c)–(m) Chromitite in the mantle diopsidite. (a,b) Chromite grains with skeletal margin, which is associated with chlorite. The silicate matrix is mainly composed of uvarovite (brighter) and anorthite (darker). (c)–(e) Chromitite filling the interstice of coarse diopside grains in the mantle diopsidite. Chromite is intergrown with grossular. Note the complicated texture of the chromite grains. (f) Chromite-grossular aggregated filling the interstice of diopside grains. Chromite is intricately mixed with silicates (mainly grossular). (g) Chromite frequently composed of the smooth core and the margin complicatedly mixed with grossular. (h) Chromite grains with complex textures. (i) Skeletal chromite grains associated with chlorite. (j) Chromite grain with globular grossular inclusions. (k) Heazlewoodite inclusions in chromite. (l) Heazlewoodite associated with grossular in chromite. (m) Chalcopyrite associated with grossular in the matrix. Abbreviations: Dio = diopside, Chr = chromite, Grs = grossular, and Chl = chlorite. Reflected light except of (c) (transmitted plane-polarized light), (d) (transmitted crossed polarized light), and (h) (BSE image).

The chromitite segregations in the mantle diopsidite [20] show a peculiar appearance (Figures 3b–d and 4c). Aggregates of fine black chromite grains (mostly less than 0.1 mm across) fill the interstice of euhedral coarse pale-greenish diopside (less than 1 cm in dimension) (Figure 3b,c and Figure 4c). The chromite is associated with grossular in the diopside interstice (Figure 4b–f). Individual chromite grains are opaque in thin section and rounded to euhedral in shape (Figure 4c,h). Some of them are in part hollow inside to various extents; the hollow part is composed of grossular or chlorite with or without vermicular chromite (Figure 4h,i and Figure 5d,e). At an extreme case, chromite shows vermicular forms: chromite strings apparently trace euhedral chromite forms within grossular or chlorite (Figure 4h,i and Figure 5e). The grossular matrix is faintly birefringent and oscillatory-zoned in a backscattered image (Figure 5d,e). The chromite grains contain abundant minute inclusions of grossular (Figure 4i). No PGM have been recognized in a thin section, even though carefully searched for. Instead, heazlewoodite is sometimes associated with chromite (Figure 4k,l). Chalcopyrite occasionally fills interstices of the matrix euhedral grossular (Figure 4m).

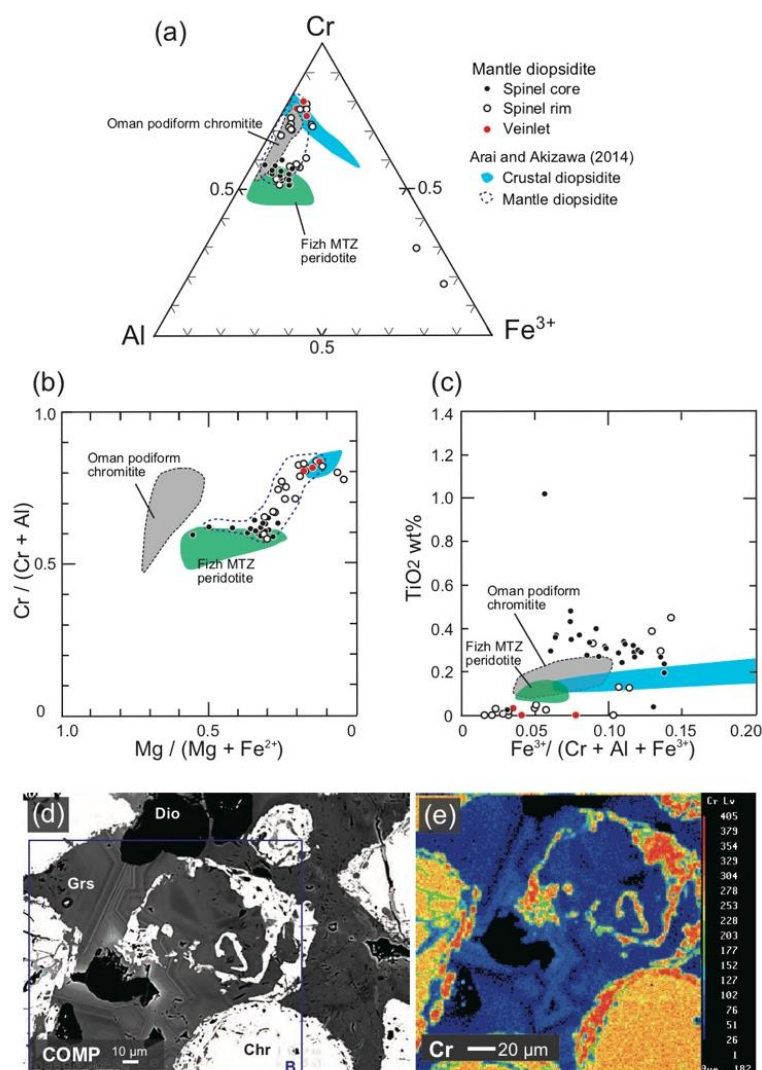


Figure 5. Chemical characteristics of chromites. (a) Trivalent cation ratios. (b) Relationship between Mg# and Cr#. (c) Relationship between Y_{Fe} and TiO₂ wt%. (d) BSE image of chromite (Chr) and surrounding grossular (Grs) in chromitite in the mantle diopsidite. (e) Distribution of Cr in a rectangular part of (d). Note the high-Cr# character of the rim/skeletal part of chromite and oscillatory zoning of the surrounding grossular.

It is interesting to note that the mineral assemblage of the hydrothermal chromitites and surrounding diopsidites from Oman is essentially the same as that of some low-temperature (<600 °C) metamorphic rocks which contain relic chromite from regional metamorphic belts [35–38]. At these metamorphic conditions, relic chromites are associated with Cr-bearing silicates, such as clinopyroxene (diopside to kosmochlor), uvarovite, chlorite, tremolite, pumpellyite, and epidote.

4. Mineral Chemistry

Mineralogical characteristics of diopsidite with or without chromite are described in detail by Arai and Akizawa [21], Akizawa and Arai [22], and Akizawa et al. [25], and summarized below. Analysis was made with a JEOL microprobe (JXA-8800R Superprobe) at Kanazawa University, Japan. Refer to Arai and Akizawa [20] for details of the analysis. Cr#, Mg#, and Y_{Fe} are Cr/(Cr + Al), Mg/(Mg + Fe²⁺), and Fe³⁺/(Cr + Al + Fe³⁺) atomic ratios, respectively. Fe²⁺ and Fe³⁺ in chromite were calculated assuming spinel stoichiometry. All Fe in Ca-rich garnets and epidotes was treated as Fe³⁺, and as Fe²⁺ in the other silicates. Selected analyses are listed in Table 1. New analysis was made only for the mantle hydrothermal chromitite here.

Table 1. Selected microprobe analyses of minerals.

Rock	Crustal Diopsidite				Mantle Diopsidite						D.L.
Mineral	chr	chr	chr	chr	chr	chr	diop	gros	gros	chl	
Note	core	rim	core	rim	verm	vein	core	core*	core	core	
SiO ₂	0.81	0.23	0.00	0.14	0.23	0.24	56.07	38.69	40.41	35.42	0.010
TiO ₂	0.16	0.25	0.32	0.03	0.00	0.03	0.02	0.15	0.05	0.00	0.015
Al ₂ O ₃	9.01	6.75	18.05	12.04	8.12	9.04	0.82	16.58	20.97	8.10	0.010
Cr ₂ O ₃	55.02	46.28	42.40	52.50	50.34	55.70	0.32	7.84	2.24	6.35	0.030
Fe ₂ O ₃	1.39	13.68	7.87	3.89	7.56	2.62	-	0.74	0.55	-	
FeO	28.62	28.88	24.87	25.82	27.28	27.84	0.77	-	-	4.58	0.020
MnO	0.55	0.59	0.53	0.72	1.23	1.14	0.00	0.02	0.04	0.13	0.017
MgO	2.6	2.33	6.63	5.21	3.16	3.41	17.90	0.03	0.04	34.34	0.008
CaO	0.29	0.11	0.05	0.34	0.51	0.43	25.56	36.64	37.23	0.04	0.009
Na ₂ O	-	0.04	0.00	0.00	0.00	-	0.06	0.00	0.00	0.02	0.011
K ₂ O	-	-	0.00	0.01	0.00	-	0.00	0.00	0.00	0.00	0.007
NiO	0.04	0.05	0.18	0.06	0.01	-	0.06	0.00	0.00	0.00	0.017
Total	98.6	99.2	100.89	100.76	98.43	100.45	101.59	100.69	101.53	88.97	
O=	4	4	4	4	4	4	6	12	12	28	
Si	0.029	0.008	0.000	0.005	0.008	0.008	1.993	2.970	3.008	6.709	
Ti	0.004	0.007	0.008	0.001	0.000	0.001	0.001	0.008	0.003	0.000	
Al	0.375	0.286	0.693	0.479	0.341	0.370	0.034	1.499	1.839	1.807	
Cr	1.536	1.314	1.091	1.399	1.419	1.528	0.009	0.475	0.132	0.951	
Fe ³⁺	0.037	0.370	0.193	0.099	0.203	0.068	-	0.043	0.031	-	
Fe ²⁺	0.845	0.867	0.677	0.728	0.814	0.808	0.023	-	-	0.725	
Mn	0.016	0.018	0.015	0.021	0.037	0.033	0.000	0.002	0.002	0.021	
Mg	0.137	0.125	0.322	0.262	0.168	0.176	0.948	0.004	0.004	9.689	
Ca	0.011	0.004	0.002	0.012	0.019	0.016	0.973	3.012	2.968	0.008	
Na	-	0.003	0.000	0.000	0.000	0.000	0.004	0.000	0.000	0.006	
K	-	0.000	0.000	0.001	0.000	0.000	0.000	0.000	0.000	0.001	
Ni	0.001	0.001	0.005	0.002	0.000	0.000	0.002	0.000	0.000	0.000	
Total	2.997	3.002	3.004	3.007	3.010	3.008	3.987	8.013	7.988	19.916	
Mg#	0.139	0.126	0.322	0.264	0.171	0.179	0.977	0.079	0.125	0.930	
Cr#	0.804	0.821	0.612	0.745	0.806	0.805	-	0.241	0.067	-	
Y _{Cr}	0.789	0.667	0.552	0.708	0.835	0.777	-	0.236	0.066	-	
Y _{Al}	0.192	0.145	0.350	0.242	0.208	0.188	-	0.743	0.919	-	
Y _{Fe}	0.019	0.188	0.098	0.050	1.043	0.035	-	0.021	0.015	-	

D.L. = detection limits (wt%); chr = chromite; diop = diopside; gros = grossular; verm = vermicular; chl = chlorite; vein, forming veinlet (Figure 3b); *, Cr-rich; -, below the detection limit; Y_{Cr} = Cr/(Al + Cr + Fe³⁺) atomic ratio; Y_{Al} = Al/(Al + Cr + Fe³⁺) atomic ratio; Y_{Fe} = Fe³⁺/(Al + Cr + Fe³⁺) atomic ratio.

4.1. Chromites

Chromitites or chromite concentrations in diopsidites are essentially similar in mineral chemistry to the host diopsidites [21]. The chemical characteristics of chromite are summarized in Figure 5. It is interesting to note that the chromite of hydrothermal origin is high in Cr# and relatively low in Y_{Fe} , similar in Cr-Al-Fe³⁺ ratios to chromites in ordinary podiform chromitites from the MTZ/mantle from the Oman ophiolite and other ophiolitic complexes [4,8,21,25,39] (Figure 5a). The Mg# is lower than 0.5, clearly lower than in the ordinary deep-seated podiform chromitites, where the Mg# is mostly > 0.5 [21] (Figure 5b). TiO₂ content of chromite is low, <0.5 wt%, in all the hydrothermal chromites from Wadi Fizh [21,25] and as low as that in the ordinary podiform chromitites (Figure 5c).

The Cr# of chromite is slightly higher than 0.8 in the crustal diopsidite (Figure 5a). The Y_{Fe} is very low (<0.05) but increases up to 0.3 at the rim in some chromite grains there [21,25] (Figure 5a). The Mg# of the crustal chromite is characteristically low, <0.2 [20] (Figure 5b). Minute chromite inclusions in uvarovite show slightly lower Cr# (0.77–0.78) and higher Mg# (0.2–0.3) [25].

The chromites in the mantle diopsidite shows clear chemical heterogeneities [21,25]. Their core shows very complicated shapes, suggesting embayment by corrosion (Figure 5d of [25]), and is relatively low in Cr# and high in Mg#, around 0.5–0.6 and 0.3–0.5, respectively [21] (Figure 5a,b). It is similar in composition to chromites in chromitites from the MTZ to the upper mantle section of Wadi Fizh of the Oman ophiolite [21] (Figure 5a,b). The mantle to marginal part around the core exhibits higher Cr#, 0.7 to 0.8, and lower Mg#, 0.3 to 0.2 [21,25]. The vermicular chromite and the chromite forming the chromitite veinlet (Figure 3b) are especially high in Cr# (>0.8) and low in Mg# (<0.2) (Figure 5a,b). The high-Cr# (>0.7) chromite tends to be high in MnO (up to 2 wt%) (Table 1). Those “peripheral” chromites are low in TiO₂ (Figure 5c). It is noteworthy that the veinlet chromite (Figure 3b) is similar in chemistry to the chromite in the crustal diopsidite (Figure 5).

4.2. Silicates

Clinopyroxenes in the crustal diopsidites are intermediate in chemistry between those in ordinary mantle diopsidites [23] and those in crustal layered gabbros [24]. They are low both in Cr₂O₃ (< 0.6 wt%; mostly 0.2 wt%) and in Na₂O (0.3 wt%) [24]. The most magnesian one, (Mg#, 0.97), is very low in Al₂O₃ (<1 wt%) and other elements and is close to the end member diopside [24]. Clinopyroxenes in the mantle diopsidite are very high in Mg# (mostly > 0.95) and contain variable amounts of Al₂O₃ (nil to 3 wt%) and Cr₂O₃ (nil to 2 wt%) [22,25]. The Na₂O content of the diopside is low, mostly < 0.2 wt%, in the mantle diopsidite, even in the Cr-rich ones. The most Cr-rich (2.3 wt% Cr₂O₃) contains 0.21 wt% Na₂O [21]. This means Cr in the diopsides is contained not as kosmochlor but as Cr-tschermakite components [25].

The uvarovite garnets in the crustal diopsidite show the Cr# higher than 0.5, which is especially high (~0.8) when coexisting with chromite [21] (Figure 6). Uvarovite component in the grossular garnets in the mantle diopsidite is up to 30 mol% [21,25] (Figure 6). The grossular in the mantle hydrothermal chromitite shows weak oscillatory zoning in terms of Cr# (Figure 5d,e). All the garnets examined are low in andradite component (<10 mol%). Both the uvarovites and grossulars examined by us show around 100 wt% oxide totals, suggesting they are almost anhydrous [21,25].

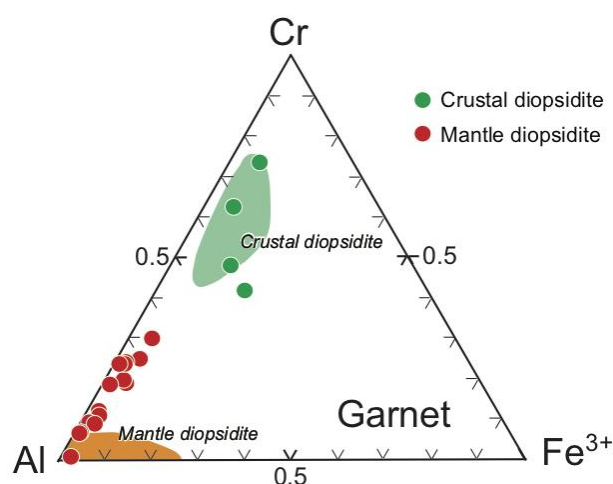


Figure 6. Cr-Al-Fe³⁺ atomic ratio of garnets associated with chromite in diopsidites. The two fields are after Arai and Akizawa [21], Akizawa and Arai [22], and Akizawa et al. [23].

All the chlorites analyzed are classified as clinocllore, according to Hey [40]. They are highly magnesian; the Mg# is 0.92 to 0.93 in the crustal diopsidite and 0.95 to 0.97 in the mantle diopsidite [25]. The Cr₂O₃ content of chlorite is around 2 wt% in the crustal diopsidite and from 3 to 5 wt% in the mantle diopsidite [24].

Other silicates in the crustal diopsidite are characterized by high Ca contents [25]. Titanites contain up to 1.2 wt% Cr₂O₃. Epidotes are high in clinozoisite component, Al/(Al + Fe³⁺ + Mn) atomic ratio being 0.89 to 0.97. Their Cr₂O₃ content is variable, at 0.1 to 2.1 wt%. Pumpellyites are relatively low in Mg#, 0.78–0.79, and, in Cr₂O₃ content, are 0.10–0.69 wt%. The An content of anorthite in the crustal diopsidite (or anorthosite) is very high, at > 0.95 [24].

5. Platinum-Group Element (PGE) Geochemistry

5.1. Bulk-Rock PGE + Re Geochemistry

Bulk-rock concentrations of PGE (Os, Ir, Ru, Pt, and Pd) and Re were determined with isotope dilution-mass spectrometry following a protocol of Ishikawa et al. [41]. The sample aliquots were digested and diluted into a 2 mL 1% HCl with spike solutions following a flow chart of Ishikawa et al. [41]. Osmium concentrations were determined by a Thermo Scientific Triton plus negative thermal ionization mass spectrometer (N-TIMS) at Tokyo Institute of Technology, Tokyo, Japan, whereas the other elemental concentrations were determined by a Thermo Scientific Element XR high resolution-inductively coupled plasma-mass spectrometer (HR-ICP-MS) at the University of Tokyo, Tokyo, Japan. The average total procedural blank compositions with one standard deviation are 0.30 ± 0.01 pg Os, 0.9 ± 0.4 pg, 4.8 ± 0.2 pg Ir, 29.9 ± 17.0 pg Pt, 2.5 ± 1.3 pg Pd, and 2.0 ± 0.2 pg Re (number of analyses is 3). All the analyses were blank corrected. The analytical results are given in Table 2.

Table 2. Bulk PGE and Re compositions of the samples.

Name	Rock Type	Sample Mass (G)	Os	Ir	Ru	Pt	Pd	Re
F-1-(X + 45) m BC (%)	Harz	0.568	5.61 0.01	3.98 0.04	8.24 0.1	12.9 0.4	5.56 0.1	0.012 22.2
20110307-2 BC (%)	Dun harz	0.512	6.72 0.01	3.09 0.1	15.9 0.1	11.4 0.5	13.1 0.04	0.0052 42.3
20121118MD pre BC (%)	MD	0.504	10.1 0.01	4.20 0.04	16.6 0.1	8.33 0.7	0.54 0.9	BDL
20090220 479 BC (%)	Gabbro	0.507	0.021 2.8	0.028 6.2	0.005 66.5	1.02 5.5	0.283 1.7	0.196 1.93
20101129 CDV BC (%)	CD	0.534	0.140 0.4	0.382 0.5	0.221 3.9	14.4 0.4	3.46 0.1	0.0009 79.5

Unit for PGE is (ng g^{-1}). Blank contributions (BC) of Ru in 20090220 gabbro, and Re in F-1-(X + 45) m harzburgite (harz), 20110307-2 dunitic (dun) harzburgite (harz), and 20101129 CDV crustal diopsidite (CD) are significant because of low concentration in the samples. BDL = below detection limit. MD = mantle diopsidite.

The hydrothermal chromitite (= chromite-rich part of diopsidite) from the mantle section (Figure 1) shows a PGE pattern flat to declining to Pd (Figure 7). It is similar in PGE pattern and level to the peridotites from the MTZ and mantle, as well as to a concordant podiform chromitite [42,43] (Figure 7). It is, however, relatively depleted in Pd (Figure 7). The chromite-rich diopsidite from the lower crust (Figure 1) shows a fractionated PGE pattern, increasing from Os to Pt and Pd (Figure 7). This pattern is similar to that of the lower crustal gabbro (Figure 7) and of almost all terrestrial magmas [44].

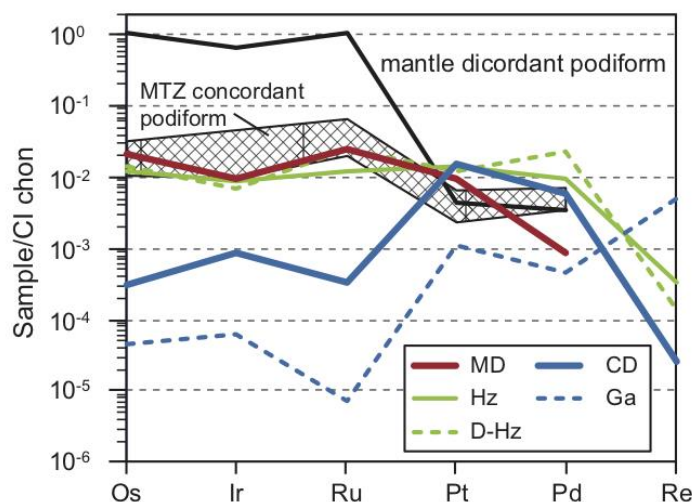


Figure 7. Chondrite-normalized platinum-group element (PGE) patterns of the hydrothermal chromitites (chromite-rich part of diopsidites) and related rocks from the northern Oman ophiolite. The patterns of podiform chromitite in the mantle and Moho transition zone (MTZ) of the Oman ophiolite are after Ahmed and Arai [42]. Chondrite values are after Fischer-Gödde et al. [45]. Abbreviations: MD = chromite-rich mantle diopsidite, Hz = harzburgite, D-Hz = dunitic harzburgite, CD = chromite-rich crustal diopsidite, and Ga = gabbro.

5.2. PGE Mineral Chemistry

As stated above, no PGM have been discovered under the microscope even though carefully looked for. The bulk total PGE contents of the hydrothermal chromitites are almost equivalent to those of a concordant podiform chromitite in the Oman mantle exposed at Wadi Hilti, which contains PGM (mainly laurite) grains visible under the microscope (Figure 7) [42,43,46].

PGE in chromite were qualitatively analyzed by LA-ICP-MS (Agilent 7500s and Microlas Geolas Q-plus) at Kanazawa University [47] to understand the distribution of PGE (or PGM) in the chromitites (Figure 8). Analyses were performed by using a spot size of 150 μm and repetition rate of 10 Hz of laser ablation with energy density of 8 J cm^{-2} (Figure 8). We measured 8 isotopes of PGE (^{101}Ru , ^{103}Rh , ^{105}Pd , ^{189}Os , ^{191}Ir , ^{192}Os , ^{193}Ir and ^{195}Pt). ^{29}Si , ^{34}S , ^{47}Ti , ^{61}Ni , ^{62}Ni , ^{63}Cu , and ^{65}Cu were also monitored for evaluation of the PGE measurement. Integrated time of 40 msec for each PGE isotope was used. Ablation for 35 s was started after measurement of the background signal for 30 s. Representative profiles of time-resolved signal count (cps: count/second) at each target spot are shown in Figures 9 and 10.

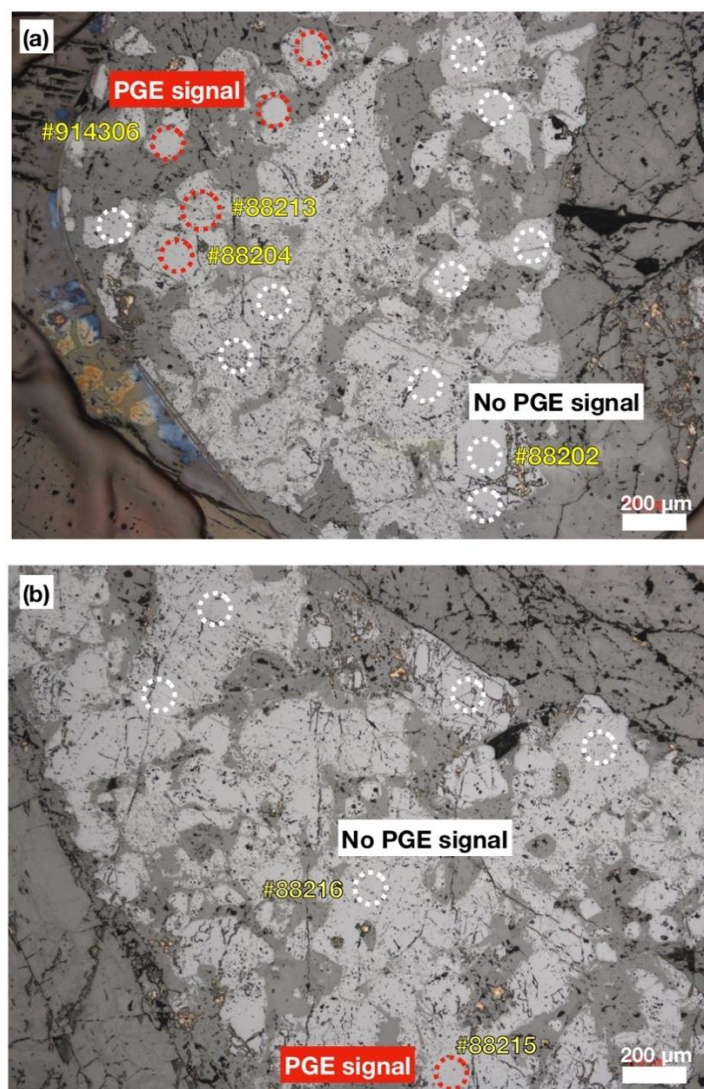


Figure 8. Examples of the LA-ICP-MS analytical spot in the chromite segregations in the mantle diopsidite. Analytical points shown in Figure 9 are labeled in yellow. The chromite grains showing PGE signals, encircled in red, are localized among those without PGE signals encircled in white. Note that chromite (brighter) is intergrown mainly with grossular (darker).

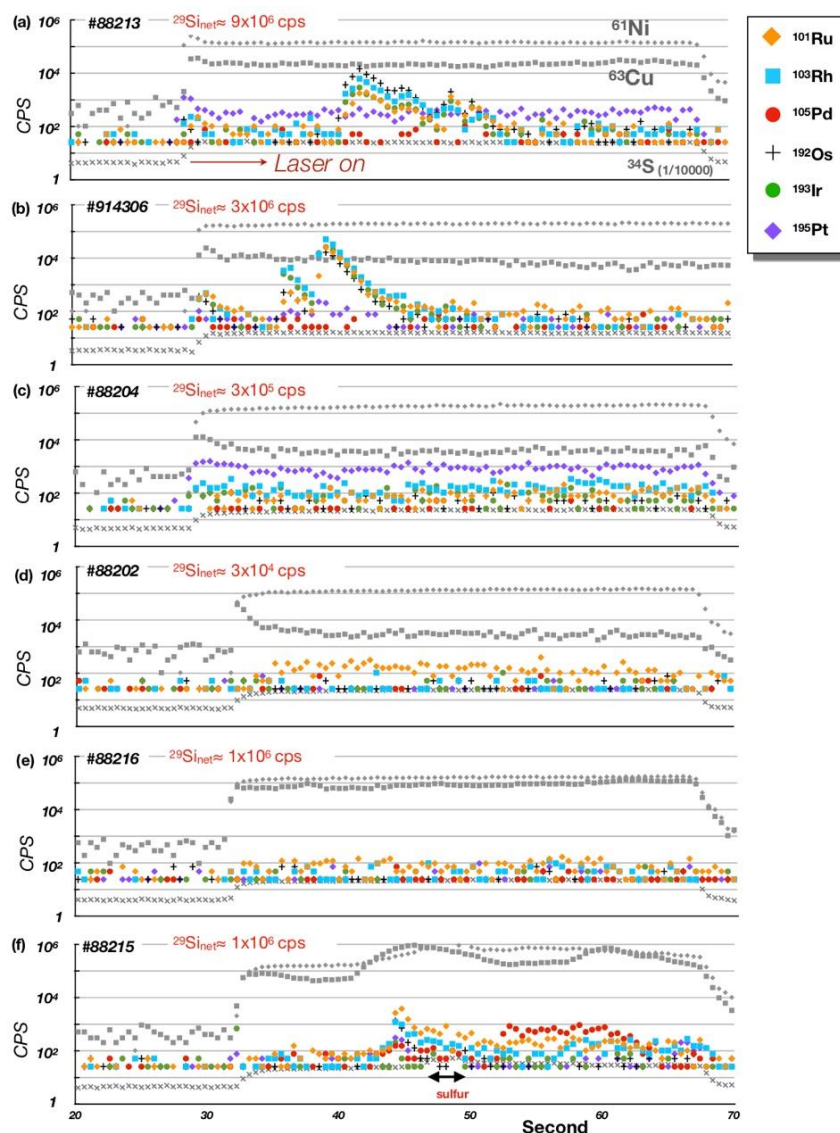


Figure 9. Profiles of time-resolved signal count (CPS: count/second) obtained by the LA-ICP-MS analysis of chromite in the chromite segregations in the mantle diopsidite at six analytical spots, (a–f): #88213 to #88215 of Figure 8. Note that wide range of $^{29}\text{Si}_{\text{net}}$ (= average (intensity in ablation–background count)) is due to garnet (grossular) contamination at each analytical spot.).

At first, we examined signal profiles of PGE isotopes in chromite in the concordant podiform chromitite (see Reference [42,43]) (Figure 10). Although signal intensities of the PGE isotope are very low (20–150 cps) as indistinguishable from the background intensity (0–25 cps) (Figure 10a), remarkable spike-like peaks of PGE isotopes were observed in the profile of some analytical spots (Figure 10b,c). Small peaks of PGE were detected with an increase in ^{63}Cu intensity in the signal profile (Figure 10b). In the ICP-MS analysis of PGE isotope, mass interference caused by oxides (MO^+) and argides (MAR^+) should be evaluated because of production of $^{61}\text{Ni}^{40}\text{Ar}^+$, $^{63}\text{Cu}^{40}\text{Ar}^+$, and $^{65}\text{Cu}^{40}\text{Ar}^+$ interferes with ^{101}Ru , ^{103}Rh , and ^{105}Pd , respectively [48]. In our measurements, the argide production rate was very low as less than 5×10^{-4} estimated from $^{101}\text{Ru}/^{61}\text{Ni}$ of NIST 610 (Figure 10d). As shown in Figure 10c, ^{103}Rh peaks can be attributed to an increase of Cu. However, ^{61}Ni is not related to an increase of ^{101}Ru . ^{192}Os and ^{193}Ir were simultaneously detected with ^{101}Ru and ^{103}Rh . ^{193}Ir can be caused by $^{176}\text{Hf}^{16}\text{O}^+$. However, no significant increase of ^{195}Pt , which is interfered by $^{179}\text{Hf}^{16}\text{O}^+$, was detected. Therefore, the mass interference of the oxide (HfO^+) can be ignored for ^{193}Ir . Although oxide interferences to

^{192}Os by production of YbO^+ , LuO^+ , and HfO^+ cannot be evaluated further, the spike of PGE isotopes in the profile indicates the presence of some PGE (as PGM) in the concordant podiform chromitite. The PGM may be alloys containing base metals.

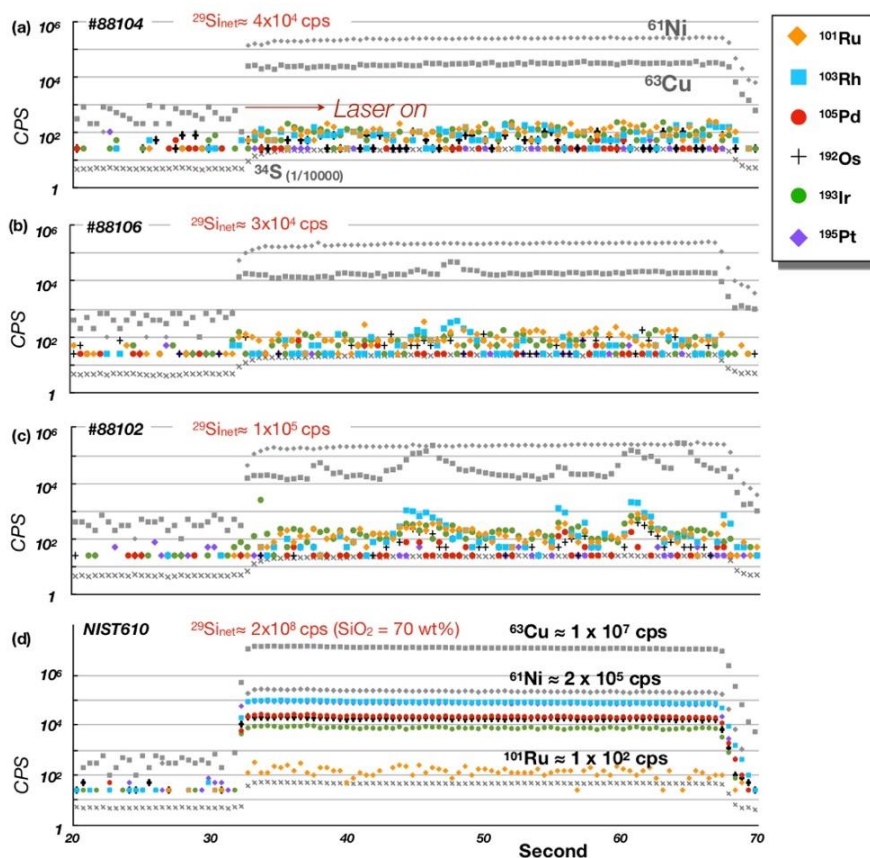


Figure 10. Profiles of time-resolved signal count (CPS: count/second) obtained by the LA-ICP-MS analysis of chromite in the concordant chromitite. (a–c) Signal profiles at three analytical spots (#88104, #88106 and #88102), respectively. Signal profiles of NIST 610 are shown in (d) for comparison. Note that concentrations of Rh, Pd and Pt in NIST 610 are reported 1.3, 1.1, and 3.2 $\mu\text{g/g}$, respectively (GeoReM database [49]). $^{29}\text{Si}_{\text{net}}$ = Average (intensity in ablation–background counts).

Similar spike-like peaks of the four PGE isotopes, such as ^{101}Ru , ^{103}Rh , ^{191}Ir , and ^{192}Os , are characteristically seen in the signal profile of the chromitite segregations in the mantle diopsidite (Figure 9). In contrast to the profiles from the concordant chromitite (Figure 10), PGE peaks are not related with fluctuation of Cu (Figure 9). While ^{95}Pt and ^{105}Pd intensities are low (10 – 10^2 cps) and constant, the highest peak intensities of the 4 PGE isotopes are exceeding 10^4 cps, which is almost equivalent to intensity of ^{63}Cu .

In the analysis of the chromitite in the mantle diopsidite, spots mixed between chromite and garnet (grossular) were also measured. The wide range of Si intensity (defined by $^{29}\text{Si}_{\text{net}}$) is mainly due to contamination of garnet (Figure 9). Assuming that the ^{29}Si intensity of chromite in the concordant chromitite (3 – 10×10^4 cps) corresponds to < 0.01 wt% of SiO_2 , spot #88213 of the mantle diopsidite corresponds to < 3 wt% of SiO_2 based on the ^{29}Si intensity (9×10^6 cps) (Figure 9a). On the other hand, #88202 and #88204 are low as equivalent to chromite in the concordant podiform chromitite in terms of Si intensity (10^4 – 10^5 cps) (Figure 9c,d). As seen in signal profiles of #88213 and #88204 (Figure 9a,c), interestingly, ^{195}Pt was constantly detected. The intensity is clearly high (10^2 – 10^3 cps) relative to the background count (0 – 50 cps). As mentioned above, HfO^+ interferes not only with ^{195}Pt but also with ^{193}Ir . Even if Hf is accommodated in the garnet and it causes interference by HfO^+ , #8813 and #88216

should be 300 and 33 times higher in ^{195}Pt than #88204, respectively. Accordingly, high ^{195}Pt at these analytical spots is not due to mass interference, and these spot data reflect that Pt is heterogeneously distributed in the hydrothermal chromitite in the mantle diopsidite.

The profile of #88215 also shows a similar spike-like peak of PGE isotopes (Figure 9f). ^{61}Ni and ^{65}Cu are considerably fluctuated through the analysis and they are increasing at the PGE peak. Sulfur was characteristically detected with the peak. On the other hand, high ^{105}Pd interval was remarkably observed after the peak. Because this interval is not dependent on the high-Cu interval, interference of $^{65}\text{Cu}^{40}\text{Ar}^+$ can be excluded. Therefore, this indicates that Pd was detected in the analytical spot.

In summary, in the hydrothermal chromitite in the mantle diopsidite the so-called IPGE (Ir-subgroup; Os, Ir, and Ru) may be present as micro-nugget of alloys in chromite, which are not visible under the microscope. In contrast, Pt and Pd (especially Pt) are more evenly distributed, either as micro-nuggets or in chromite structure, in some chromite grains independently of the IPGE micro-nuggets.

6. Discussion

6.1. Role of H_2O in the Podiform Chromitite Formation

Chromitites in peridotitic rocks, such as podiform chromitites, are most commonly suffered from severe selective hydration. This has led us to make misunderstanding of the role of water in chromitite genesis. As stated in Arai [16], the selective hydration around chromitite is due to a highly magnesian character of olivine in the chromitite and its dunite envelope. If the chromitite is cooled with successive water supply, the dunitic matrix of chromitite and surrounding dunite, of which olivines have been enriched in Mg via Mg-Fe redistribution with chromite, will be preferentially altered at higher temperature than ambient peridotites [50] (Figure 11). This apparently selective settling of water in and around chromitite is one of subsolidus phenomena due to high concentrations of chromite, but the water supply is not essentially related to the primary concentration of chromite [16] (Figure 11). This can occur in a microscopic way in peridotites, where the olivine has been selectively hydrated around chromian spinel (Figure 12). This is in part due to a reaction between chromian spinel and olivine to form chlorite at some higher temperatures prior to initiation of serpentinization [16]. In conclusion, the selective serpentinization or chloritization in and around chromitite is not the evidence for involvement of water in primary formation of chromitite.

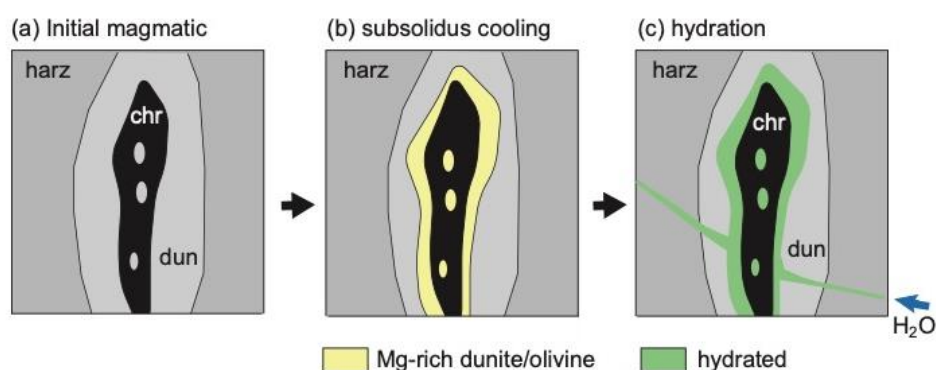


Figure 11. Cartoon to show the selective hydration in and around chromitite (chr) pod in dunite (dun). Olivines in and around chromitite have been enriched in Mg (b) after magmatic formation (a), and then the Mg-rich part of the olivine has been selectively hydrated (serpentinized) (c) due to the high-Mg character. harz = harzburgite.

The presence of hydrous silicate inclusions in chromite is possibly not related to concentration of chromite for chromitite. The chromite-hosted silicate inclusions, which represent trapped melt rich in water and Na, are also commonly found in dunites, troctolites, and related rocks from the current

ocean floor [51–53], in addition to chromitites [51,54,55]. The formation of troctolites and dunites from mantle harzburgite is closely associated with dissolution of mantle orthopyroxene via reaction with an invading magma [51,56]. The reaction between the mantle orthopyroxene and exotic melt from deeper part produces chemically heterogeneous secondary melt, of which some part is rich in silica and alkalis [57]. Peridotite-magma reaction is also one of the important elements of podiform chromitite formation [8]. We suggest that the presence of chromite-hosted hydrous inclusions is not directly related with the chromite concentration process. And, again, it does not provide any evidence for the involvement of hydrothermal fluids in podiform chromitite formation.

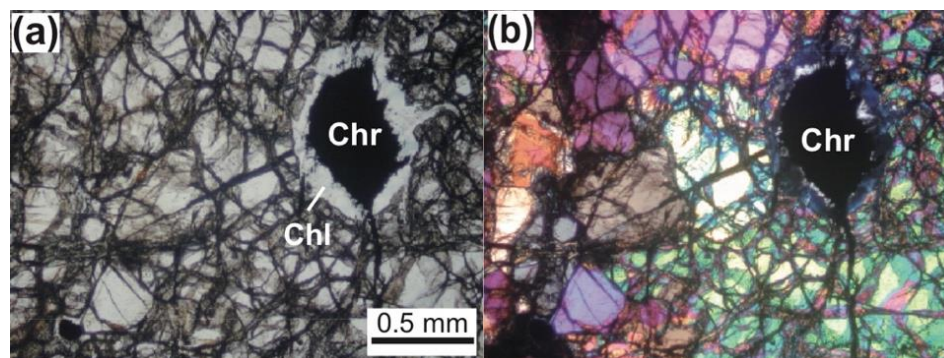


Figure 12. Photomicrographs of chlorite corona around primary chromian spinel in otherwise fresh peridotite from Ochiai-Hokubo peridotite complex, southwestern Japan [58]. Note the selective hydration of olivine around the spinel, which is due to selective Mg-enrichment of olivine around spinel, as well as to selective reaction between spinel and surrounding olivine. (a) Plane-polarized light. (b) Crossed-polarized light. Chr = chromian spinel; Chl = chlorite.

Hydrothermal fluids modify the chemical composition of chromites to various degrees. Both the addition of magnetite component on decomposition of olivine (and formation of serpentine) and the subtraction of spinel (MgAl_2O_4) component on formation of chlorite may form secondary chromites rich in Cr, Fe^{2+} and Fe^{3+} [26]. No petrographical and textural evidence for precipitation of those high-Cr, -Fe chromites directly from hydrothermal fluids.

6.2. Precipitation and Concentration of Chromites from Hydrothermal Fluids

Both dissolution and precipitation of chromites from hydrothermal fluids were recognized in the Oman ophiolite by Arai and Akizawa [21], Akizawa and Arai [22], and Akizawa et al. [25]. Concentration of the hydrothermal chromites was also clearly shown by those authors. The temperature of the hydrothermal chromitite formation of Oman is possibly 700–800 °C, according to the critical mineral assemblage (anorthite-diopside-chlorite) and mineral chemistry [21,23,25]. Some of the minerals in the diopsidites and related chromities are possibly of retrograde origin.

The seam-like segregation of chromite at the interstice of coarse euhedral diopside in the mantle diopsidite indicates that a chromite-oversaturated fluid got formed by fractional crystallization of diopside (Figure 2). The dendritic or skeletal form of chromite (Figure 3) in chromitite suggests chromite oversaturation after fast precipitation of large amounts of diopside from the fluid. After the diopside production, Cr-bearing grossular is co-precipitated with chromite [22]. The thin chromitite veinlet branching from the main segregations (Figure 3b) in diopsidite indicates injection of the chromite-oversaturated fluid into the early-formed wall diopsidite. The seam-like chromitite segregations are present around the central part of the thickest part of diopsidite (Figure 1e of Reference [21]), possibly indicating the chromite-oversaturated fluid was produced after precipitation of diopside from the peridotite walls both upward and downward.

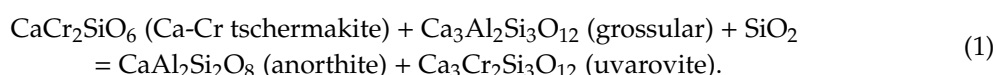
The core of chromite grains of the hydrothermal chromitite in the mantle diopsidite is similar in chemistry to chromites in podiform chromitites or peridotite from Oman (Figure 5a–c). Combined

with the textural character of the core chromite (Figures 4 and 5d,f), it possibly represents relics of mantle chromites from podiform chromitite or peridotite. This is consistent with the similar PGE pattern between the chromite-rich part of mantle diopsidite and chromitite (concordant)/peridotite (Figure 7). This further means that the mantle chromite was incorporated in the fluid before or during metasomatic precipitation of diopsidite and subsequently modified/digested in part to give rise to formation of Cr-rich fluids, which precipitated chromite during cooling. The mantle chromite was most probably incorporated from a magmatic chromitite seam in the uppermost mantle just beneath MTZ (Figure 1).

The micro-pods of chromitite in the crustal diopsidite exist in the uvarovite-rich part [21] (Figure 3a), which is enveloped by anorthosite-rich part (or anorthosite) within crustal layered gabbros. The field relation indicates that the fluid invading the gabbro first crystallized anorthite via reaction with the wall gabbro (Figure 2a,b). Cr-rich diopsidite was formed within the fluid conduit lined with anorthite-rich rocks (Figure 2a). The Cr# of the fluid fluctuated in the conduit and precipitated chromite and uvarovite when it was high and low, respectively [21]. The fluid precipitated both chromite and high-Cr# uvarovite when it was intermediate in Cr# [21]. When it was very high in Cr#, the degree of chromite-oversaturation was so enhanced that skeletal or dendritic chromite was crystallized and aggregated to form the chromitite micro-pods (Figure 3a).

The bulk-rock PGE characteristics suggest that Pd was released from the initial podiform chromitite during reaction with the fluid that dissolved chromite because of the slight drop of the PGE pattern at Pd for the mantle hydrothermal chromitite (Figure 7). The mantle hydrothermal chromitite may be representative of a residual character of a podiform chromitite when reacted with hydrothermal fluids, which can dissolve its chromite. The highly fractionated Pt-, Pd-rich pattern of the crustal hydrothermal chromitite (chromite-rich diopsidite), which is a cumulate from the hydrothermal fluid, is due to enrichment of Pt and Pd in the fluid [59–61]. The distribution of PGE in the hydrothermal chromite (Figures 8 and 9) suggests a high heterogeneity in PGE (especially Pt) in the hydrothermal fluid that is a reaction product between the circulated fluid and the primary mantle chromite. The chemically heterogeneous fluid was separated and homogenized to produce an as-a-whole high-Pt (-Pd) fluid, which could precipitate chromite with high Pt/Os ratio upsection (Figure 7).

It is noteworthy that the main Cr-containing mineral is diopside after chromite in the mantle diopsidite but is uvarovite (garnet) in the crustal diopsidite. The Cr-rich diopside coexists with grossular in the mantle section, and the uvarovite, with anorthite in the crustal section. These assemblages may be related to each other by a reaction,



The fluid involved in formation of the crustal diopsidite is higher in silica content than that for the mantle diopsidite. The crustal fluid was formed from the fluid passing through the mantle through a kind of crystallization differentiation via precipitation of the minerals of the mantle diopsidite because the two diopsidites are spatially very close to each other (about 70 m apart in stratigraphic level).

6.3. Origin of the Fluid

The fluid responsible for formation of the diopsidite + chromitite was possibly originated from the seawater, as Python et al. [23] suggested (Figure 13). Detection of Na-bearing H₂O-rich fluid from inclusions in titanite in the crustal diopsidite [25] is consistent with this idea. Chlorine and other anions may form complexes with chromium that are soluble in water-rich fluids [21,62,63]. Saline fluids are also expected to be released from the slab to the mantle wedge [64–67]. If we carefully look peridotite xenoliths derived from the mantle wedge, we frequently observe some textures suggesting accumulation of fine chromite or chromian spinel grains (Figure 14). They are mostly within olivine and sometimes form secondary inclusions trails associated with fluids and sulfide (Figure 14). We suggest that the chromite or chromian spinel of this occurrence are precipitated from aqueous fluids or highly

hydrous melts released from the slab. Precipitation of chromian spinel is observed in some peridotite xenoliths of mantle wedge origin from the Avacha volcano, Kamchatka [68]. Metasomatic addition of pyroxenes, including diopside, is also recognized in highly metasomatized peridotite xenoliths from Avacha [69]. Those mean that some of the fluids derived from the slab possibly precipitate chromite or chromian spinel and Ca-rich silicates in the mantle. The fluids originated from the crust obtain calcium and aluminum when they pass through the crustal rocks, and chromium when they pass through the mantle rocks.

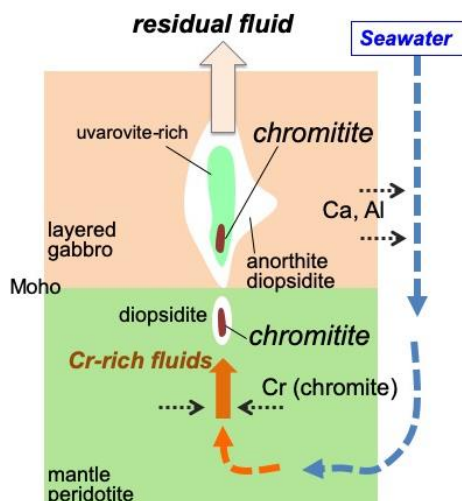


Figure 13. Illustration showing the generation of hydrothermal chromitites in the northern Oman ophiolite. Hot seawater circulating in the oceanic crust obtained Ca, Al, and other elements, and precipitated diopside both in the mantle and in the lower crust. The sea water-derived fluid dissolved/precipitated chromite during the mantle diopside formation, and precipitated chromite in the crustal diopside. Modified after Arai and Miura [4].

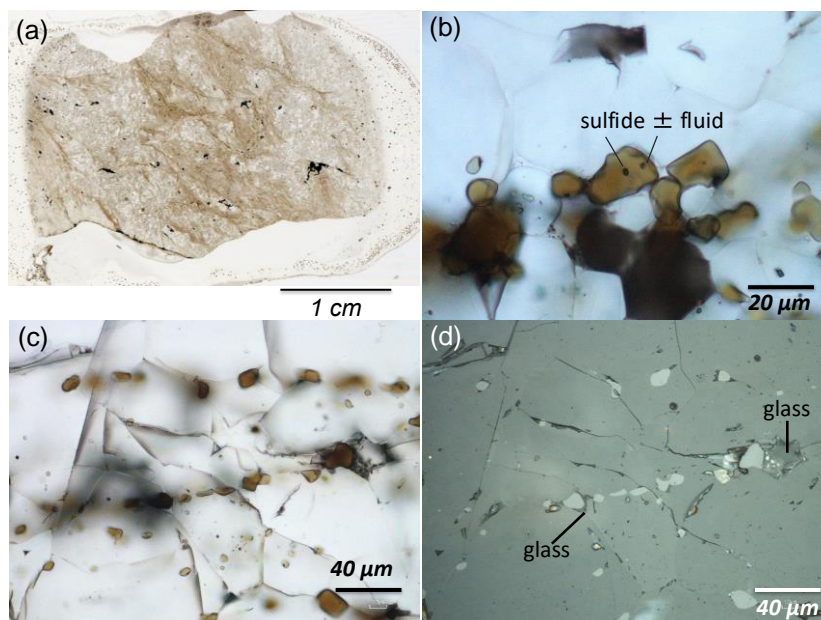


Figure 14. Fine chromite grains in a fine-grained type of peridotite xenolith from Avacha, Kamchatka. See Ishimaru et al. [64] and Ishimaru and Arai [68,69] for details. (a) Thin section. Note the brown-colored fine-grained chromite-rich part in addition to black discrete primary chromite. (b–d) Photomicrographs of the fine chromite grains. (b) Chromite grains containing sulfide and fluid inclusions. (c) Fine chromite grains forming trails. (d) Reflected light image. Spinel grains are closely associated with glass.

7. Conclusions

Hydrothermal chromitites can be formed from water-rich fluids, both in the crust and in the mantle. The aqueous fluids are saline, being derived either from the seawater or from the subducting slab. Chromitites are precipitated from such Cr-rich saline aqueous fluids on transportation upward because of drop of Cr solubility on decompression and/or cooling of the fluids [63], possibly similar to the magmatic chromite precipitation in magma chamber [70]. If a sudden decrease in oxygen fugacity is available in the saline fluids [71], chromite is also possibly concentrated from the fluids. The hydrothermal chromitites are characterized by the association of Ca-Al silicates, such as diopside and Ca-garnets. They are in contrast to magmatic podiform chromitites, of which silicate matrix is mainly composed of olivine. The fluid possibly redistributes chromium and chromite (or chromian spinel) within the mantle wedge significantly, where saline aqueous fluids are possibly circulating [67]. It can mobilize Pt and Pd in the mantle wedge and crust significantly, although we need more data and information on this subject.

Author Contributions: Conceptualization, S.A.; field work, S.A., M.M. and N.A.; microprobe analysis, M.M. and N.A.; LA-ICP-MS analysis, A.T.; bulk PGE analysis, N.A. and A.I.; data curation, S.A., M.M., A.T. and N.A.; writing—review and editing, S.A.; project administration, S.A.; funding acquisition, S.A. All authors have read and agreed to the published version of the manuscript.

Funding: This research was funded by Monkasho Special Budget Project No. 812000009 to S. Arai.

Acknowledgments: We thank M. Takeuchi, J. Uesugi, S. Ishimaru, H. Negishi, M. Python, A. Perez and C. Hoshikawa for their collaborations in the field. T. Morishita supported us in our laboratory analyses at Kanazawa University. We are grateful to Salim Al-Ibrahim, Mahommed Al-Battashi, Mohamed Al-Araimi of Ministry of Commerce and Industry of Oman for their support in our field work in the Oman ophiolite. Comments of two anonymous reviewers were helpful in revision.

Conflicts of Interest: The authors declare no conflict of interest.

References

- Irvine, T.N. Chromian spinel as a petrogenetic indicator. Part II. Petrogenetic applications. *Can. J. Earth Sci.* **1967**, *4*, 72–103. [\[CrossRef\]](#)
- Thayer, T.P. Principal features and origin of podiform chromitite deposits, and some observations on the Guleman-Soridag district, Turkey. *Econ. Geol.* **1964**, *59*, 1497–1524. [\[CrossRef\]](#)
- Cassard, D.; Nicolas, A.; Rabinovitch, M.; Moutte, J.; Leblanc, M.; Prinzhofer, A. Structural classification of chromite pods in southern New Caledonia. *Econ. Geol.* **1981**, *76*, 805–831. [\[CrossRef\]](#)
- Arai, S.; Miura, M. Formation and modification of chromitites in the mantle. *Lithos* **2016**, *264*, 277–295. [\[CrossRef\]](#)
- Jackson, E.D. The chromite deposits of the Stillwater Complex, Montana. In *Ore Deposits of the United States, 1933–1967; The Graton-Sales Volume 2*; Ridge, J.D., Ed.; The American Institute of Mining, Metallurgical, and Petroleum Engineers, Inc.: New York, NY, USA, 1968; pp. 1495–1510.
- Irvine, T.N.; Smith, C.H. Primary oxide minerals in the layered series of the Muskox intrusion. In *Magmatic Ore Deposits*; Wilson, H.D.B., Ed.; Economic Geology Publishing Co.: New Haven, CT, USA, 1969; pp. 76–94.
- Schulte, R.F.; Taylor, R.D.; Piatak, N.M.; Seal, R.R., II. Stratiform Chromite Deposit Model: Chapter E in Mineral Deposit Model for Resource Assessment. U.S. In *Geological Survey Scientific Investigation Report 2010-5070-E*; U.S. Geological Survey: Reston, VA, USA, 2012; p. 131.
- Arai, S.; Yurimoto, H. Podiform chromitites of the Tari-Misaka ultramafic complex, southwestern Japan, as mantle-melt interaction products. *Econ. Geol.* **1994**, *89*, 1279–1285. [\[CrossRef\]](#)
- Johan, Z.; Dunlop, H.; Le Bel, L.; Robert, J.-L.; Volfinger, M. Origin of chromite deposits in ophiolitic complexes: Evidence for a volatile- and sodium-rich reducing fluid phase. *Fortsch. Mineral.* **1983**, *61*, 105–107.
- Johan, Z.; Martin, R.F.; Ettler, V. Fluids are bound to be involved in the formation of ophiolitic chromite deposits. *Eur. J. Mineral.* **2017**, *29*, 543–555. [\[CrossRef\]](#)
- McElduff, B.; Stumpfl, E.F. The chromite deposits of the Troodos complex, Cyprus—evidence for the role of a fluid phase accompanying chromite formation. *Mineral. Depos.* **1991**, *26*, 307–318. [\[CrossRef\]](#)

12. Matveev, S.; Ballhaus, C. Role of water in the origin of podiform chromitite deposits. *Earth Planet. Sci. Lett.* **2002**, *203*, 235–243. [[CrossRef](#)]
13. Borisova, A.Y.; Ceuleneer, G.; Kamenetsky, V.S.; Arai, S.; Bějina, F.; Abily, B.; Bindeman, I.N.; Polvé, M.; De Parseval, P.; Aigouy, T.; et al. A new view on the petrogenesis of the Oman ophiolite chromitites from microanalyses of chromite-hosted inclusions. *J. Petrol.* **2012**, *53*, 2411–2440. [[CrossRef](#)]
14. Rospabé, M.; Ceuleneer, G.; Granier, N.; Arai, S.; Borisova, A. Multi-scale development of a stratiform chromite ore body at the base of the dunitic mantle-crust transition zone (Maqsad diapir, Oman ophiolite): The role of repeated melt and fluid influxes. *Lithos* **2019**, *350*, 105235. [[CrossRef](#)]
15. Pushkarev, E.V.; Kamenetsky, V.S.; Morozova, A.V.; Khiller, V.V.; Glavatskykh, S.P.; Rodemann, T. Ontogeny of ore Cr-spinel and composition of inclusions as indicators of the pneumatolytic-hydrothermal origin of PGM-bearing chromitites from Kondyor massif, the Aldan Shield. *Geol. Ore Depos.* **2015**, *57*, 352–380. [[CrossRef](#)]
16. Arai, S. Formation of chlorite corona around chromian spinel in peridotite and its significance. *Geosci. Rep. Shizuoka Univ.* **1978**, *3*, 9–15. (In Japanese)
17. González-Jiménez, J.M.; Kerestedjian, T.; Proenza, J.A.; Gervilla, F. Metamorphism on chromite ores from the Dobromirski ultramafic massif, Rhodope Mountains (SE Bulgaria). *Geol. Acta* **2009**, *7*, 413–429.
18. Fisher, L.W. Origin of chromite deposits. *Econ. Geol.* **1929**, *24*, 691–721. [[CrossRef](#)]
19. Ross, C.S. The origin of chromite. *Econ. Geol.* **1931**, *26*, 540–545. [[CrossRef](#)]
20. Sampson, E. Varieties of chromite deposits. *Econ. Geol.* **1931**, *26*, 833–839. [[CrossRef](#)]
21. Arai, S.; Akizawa, N. Precipitation and dissolution of chromite by hydrothermal solutions in the Oman ophiolite: New behavior of Cr and chromite. *Am. Mineral.* **2014**, *99*, 28–34. [[CrossRef](#)]
22. Akizawa, N.; Arai, S. Petrology of mantle diopsidite from Wadi Fizh, northern Oman ophiolite: Cr and REE mobility by hydrothermal solution. *Island Arc* **2014**, *23*, 269–280. [[CrossRef](#)]
23. Python, M.; Ceuleneer, G.; Ishida, Y.; Barrat, J.-A.; Arai, S. Oman diopsidites: A new lithology of very high temperature hydrothermal circulation in mantle peridotite below oceanic spreading centres. *Earth Planet. Sci. Lett.* **2007**, *255*, 289–305. [[CrossRef](#)]
24. Akizawa, N.; Arai, S.; Tamura, A.; Uesugi, J.; Python, M. Crustal diopsidites from the northern Oman ophiolite: Evidence for hydrothermal circulation through suboceanic Moho. *J. Mineral. Petrol. Sci.* **2011**, *106*, 261–266. [[CrossRef](#)]
25. Akizawa, N.; Tamura, A.; Fukushi, K.; Yamamoto, J.; Mizukami, T.; Python, M.; Arai, S. High-temperature hydrothermal activities around suboceanic Moho: An example from diopsidite and anorthosite in Wadi Fizh, Oman ophiolite. *Lithos* **2016**, *263*, 66–87. [[CrossRef](#)]
26. Arai, S.; Shimizu, Y.; Ismail, S.A.; Ahmed, A.H. Low-*T* formation of high-Cr spinel with apparently primary chemical characteristics within podiform chromitite from Rayat, northeastern Iraq. *Mineral. Mag.* **2006**, *70*, 499–508. [[CrossRef](#)]
27. Kapsiotis, A.N. Alteration of chromitites from the Voidolakkos and Xerolivado mines, Vourinos ophiolite complex, Greece: Implications for deformation-induced metamorphism. *Geol. J.* **2015**, *50*, 739–763. [[CrossRef](#)]
28. Lippard, S.J.; Shelton, A.W.; Gass, I.G. The ophiolite of northern Oman. *Geol. Soc. Lond. Mem.* **1986**, *11*, 178.
29. Akizawa, N.; Arai, S. Petrologic profile of a peridotite layer under a possible Moho in the northern Oman ophiolite: An example from Wadi Fizh. *J. Mineral. Petrol. Sci.* **2009**, *104*, 389–394. [[CrossRef](#)]
30. Takazawa, E.; Okayasu, T.; Satoh, K. Geochemistry and origin of the basal lherzolites from the northern Oman ophiolite (northern Fizh block). *Geochem. Geophys. Geosyst.* **2003**, *4*, 1021. [[CrossRef](#)]
31. Ministry of Petroleum and Minerals. *Geological Map of Buraymi, Scale 1:250,000*; Ministry of Petroleum and Minerals: Muscat, Sultanate of Oman, 1992.
32. Uesugi, J.; Arai, S.; Morishita, T.; Matsukage, K.; Kadoshima, K.; Tamura, A.; Abe, N. Significance and variety of mantle-crust boundary in the Oman ophiolite. *J. Geogr. (Chigaku Zasshi)* **2003**, *112*, 750–768. (In Japanese) [[CrossRef](#)]
33. Akizawa, N.; Arai, S.; Tamura, A. Behavior of MORB magmas at uppermost mantle beneath a fast-spreading axis: An example from Wadi Fizh of the northern Oman ophiolite. *Contrib. Mineral. Petrol.* **2012**, *164*, 601–625. [[CrossRef](#)]

34. Akizawa, N.; Ozawa, K.; Tamura, A.; Michibayashi, K.; Arai, S. Three-dimensional evolution of melting, heat and melt transfer in ascending mantle beneath a fast-spreading ridge segment constrained by trace elements in clinopyroxene from concordant dunites and host harzburgites of the Oman ophiolite. *J. Petrol.* **2016**, *57*, 777–814. [\[CrossRef\]](#)
35. Treloar, P.J. The Cr-minerals of Outokumpu—Their chemistry and significance. *J. Petrol.* **1987**, *28*, 867–886. [\[CrossRef\]](#)
36. Tsujimori, T.; Liou, J.G. Coexisting chromian omphacite and diopside in tremolite schist from the Chugoku Mountains, SW Japan: The effect of Cr on the omphacite-diopside immiscibility gap. *Am. Mineral.* **2004**, *89*, 7–14. [\[CrossRef\]](#)
37. Tsujimori, T.; Liou, J.G. Low-pressure and low-temperature K-bearing kosmochloric diopside from the Osayama serpentinite mélange, SW Japan. *Am. Mineral.* **2005**, *90*, 1629–1635. [\[CrossRef\]](#)
38. Hamada, M.; Seto, S.; Akasaka, M.; Takasu, A. Chromian pumpellyite and associated chromian minerals from Sangun metamorphic rocks, Osayama, southwest Japan. *J. Mineral. Petrol. Sci.* **2008**, *103*, 390–399. [\[CrossRef\]](#)
39. Arai, S. Control of wall-rock composition on the formation of podiform chromitites as a result of magma/peridotite interaction. *Resour. Geol.* **1997**, *47*, 177–187.
40. Hey, M.H. A new review of chlorites. *Mineral. Mag.* **1954**, *30*, 277–299. [\[CrossRef\]](#)
41. Ishikawa, A.; Senda, R.; Suzuki, K.; Dale, C.W.; Meisel, T. Re-evaluating digestion methods for highly siderophile element and Os-187 isotope analysis: Evidence from geological reference materials. *Chem. Geol.* **2014**, *384*, 27–46. [\[CrossRef\]](#)
42. Ahmed, A.H.; Arai, S. Unexpectedly high-PGE chromitite from the deeper mantle section of the northern Oman ophiolite and its tectonic implications. *Contrib. Mineral. Petrol.* **2002**, *143*, 263–278. [\[CrossRef\]](#)
43. Miura, M.; Arai, S.; Ahmed, A.H.; Mizukami, T.; Okuno, M.; Yamamoto, S. Podiform chromitite classification revisited: A comparison of discordant and concordant chromitite pods from Wadi Hilti, northern Oman ophiolite. *J. Asian Earth Sci.* **2012**, *59*, 52–61. [\[CrossRef\]](#)
44. Barnes, S.-J.; Naldrett, A.J.; Gorton, M.P. The origin of the fractionation of platinum-group elements in terrestrial magmas. *Chem. Geol.* **1985**, *53*, 303–323. [\[CrossRef\]](#)
45. Fischer-Gödde, M.; Becker, H.; Wombacher, F. Rhodium, gold and other highly siderophile element abundances in chondritic meteorites. *Geochim. Cosmochim. Acta* **2010**, *74*, 356–379. [\[CrossRef\]](#)
46. Ahmed, A.H.; Arai, S. Platinum-group minerals in podiform chromitites of the Oman ophiolite. *Can. Mineral.* **2003**, *41*, 597–616. [\[CrossRef\]](#)
47. Morishita, T.; Ishida, Y.; Arai, S. Simultaneous determination of multiple trace element compositions in thin (<30 µm) layers of BCR-2G by 193 nm ArF excimer laser ablation-ICP-MS: Implications for matrix effect and elemental fractionation on quantitative analysis. *Geochem. J.* **2005**, *39*, 327–340. [\[CrossRef\]](#)
48. Park, J.-W.; Campbell, I.H.; Eggins, S.M. Enrichment of Rh, Ru, Ir and Os in Cr spinels from oxidized magmas: Evidence from the Ambae volcano, Vanuatu. *Geochim. Cosmochim. Acta* **2012**, *78*, 28–50. [\[CrossRef\]](#)
49. Jochum, K.P.; Nohl, U. Reference materials in geochemistry and environmental research and the GeoReM database. *Chem. Geol.* **2008**, *253*, 50–53. [\[CrossRef\]](#)
50. Frost, B.R. On the stability of sulfides, oxides, and native metals in serpentinite. *J. Petrol.* **1985**, *26*, 31–63. [\[CrossRef\]](#)
51. Arai, S.; Matsukage, K. Petrology of the gabbro-troctolite complex from Hess Deep, equatorial Pacific: Implications for mantle-melt interaction within the oceanic lithosphere. *Proc. ODP Sci. Results* **1996**, *47*, 135–155.
52. Tamura, A.; Morishita, T.; Ishimaru, S.; Arai, S. Geochemistry of spinel-hosted amphibole inclusions in abyssal peridotite: Insight into secondary melt formation in melt–Peridotite reaction. *Contrib. Mineral. Petrol.* **2014**, *167*, 974. [\[CrossRef\]](#)
53. Tamura, A.; Morishita, T.; Ishimaru, S.; Hara, K.; Sanfilippo, A.; Arai, S. Compositional variations in spinel-hosted pargasite inclusions in the olivine-rich rock from the oceanic crust–mantle boundary zone. *Contrib. Mineral. Petrol.* **2016**, *171*, 39. [\[CrossRef\]](#)
54. Matsukage, K.; Arai, S. Jadeite, albite and nepheline as inclusions in spinel of chromitite from Hess Deep, equatorial Pacific: Their genesis and implications for serpentinite diapir formation. *Contrib. Mineral. Petrol.* **1998**, *131*, 111–122. [\[CrossRef\]](#)

55. Arai, S.; Matsukage, K. Petrology of a chromitite micropod from Hess Deep, equatorial Pacific: A comparison between abyssal and alpine-type podiform chromitites. *Lithos* **1998**, *43*, 1–14. [[CrossRef](#)]
56. Tamura, A.; Arai, S.; Ishimaru, S.; Andal, E.S. Petrology and geochemistry of peridotites from IODP Site U1309 at Atlantis Massif, MAR 30° N: Micro- and macro-scale melt penetrations into peridotites. *Contrib. Mineral. Petrol.* **2008**, *155*, 491–509. [[CrossRef](#)]
57. Shaw, C.S.J. Dissolution of orthopyroxene in basanitic magma between 0.4 and 2 GPa: Further implications for the origin of Si-rich alkaline glass inclusions in mantle xenoliths. *Contrib. Mineral. Petrol.* **1999**, *135*, 114–132. [[CrossRef](#)]
58. Arai, S.; Shirasaka, M.; Ishida, Y.; Inoue, H. Na-bearing tremolites as reservoirs of fluid-mobile elements in the mantle wedge: Inference from the Ochiai-Hokubo complex (Southwest Japan) in high-*P* schists. *J. Mineral. Petrol. Sci.* **2019**, *114*, 231–237. [[CrossRef](#)]
59. Gammons, C.H. Experimental investigations of the hydrothermal geochemistry of platinum and palladium: V. Equilibria between platinum metal, Pt (II), and Pt (IV) chloride complexes at 25 to 300 °C. *Geochim. Cosmochim. Acta* **1996**, *60*, 1683–1694. [[CrossRef](#)]
60. Augé, T.; Petrunov, R.; Bailly, L. On the origin of the PGE mineralization in the Elastsite porphyry Cu-Au deposit, Bulgaria: Comparison with the Baula-Nuasahi complex, India, and other alkaline PGE-rich porphyries. *Can. Min.* **2005**, *43*, 1355–1372. [[CrossRef](#)]
61. Barnes, S.J.; Liu, W. Pt and Pd mobility in hydrothermal fluids: Evidence from komatiites and from thermodynamic modelling. *Ore Geol. Rev.* **2012**, *44*, 49–58. [[CrossRef](#)]
62. Oze, C.; Fendorf, S.; Bird, D.K.; Coleman, R.G. Chromium geochemistry in serpentinized ultramafic rocks and serpentine soils from the Franciscan Complex of California. *Am. J. Sci.* **2004**, *304*, 67–101. [[CrossRef](#)]
63. Watenphul, A.; Schmidt, C.; Jahn, S. Cr (III) solubility in aqueous fluids at high pressures and temperatures. *Geochim. Cosmochim. Acta* **2014**, *126*, 212–227. [[CrossRef](#)]
64. Ishimaru, S.; Arai, S.; Ishida, Y.; Shirasaka, M.; Okrugin, V.M. Melting and multi-stage metasomatism in the mantle wedge beneath a frontal arc inferred from highly depleted peridotite xenoliths from the Avacha volcano, southern Kamchatka. *J. Petrol.* **2007**, *48*, 395–433. [[CrossRef](#)]
65. Kawamoto, T.; Yoshikawa, M.; Kumagai, Y.; Mirabueno, M.H.T.; Okuno, M.; Kobayashi, T. Mantle wedge infiltrated with saline fluids from dehydration and decarbonation of subducting slab. *Proc. Natl. Acad. Sci. USA* **2013**, *110*, 9663–9668. [[CrossRef](#)] [[PubMed](#)]
66. Yoshikawa, M.; Tamura, A.; Arai, S.; Kawamoto, T.; Payot, B.D.; Rivera, D.J.; Bariso, E.B.; Mirabueno, M.H.T.; Okuno, M.; Kobayashi, T. Aqueous fluids and sedimentary melts as agents for mantle wedge metasomatism, as inferred from peridotite xenoliths at Pinatubo and Iraya volcanoes, Luzon arc, Philippines. *Lithos* **2016**, *262*, 355–368. [[CrossRef](#)]
67. Huang, Y.; Nakatani, T.; Nakamura, M.; McCammon, C. Saline aqueous fluid circulation in mantle wedge inferred from olivine wetting properties. *Nat. Commun.* **2019**, *10*, 5557. [[CrossRef](#)] [[PubMed](#)]
68. Ishimaru, S.; Arai, S. Calcic amphiboles in peridotite xenoliths from Avacha volcano, Kamchatka, and their implications for metasomatic conditions in the mantle wedge. In *Metasomatism in Oceanic and Continental Lithospheric Mantle*; Coltorti, M., Grégoire, M., Eds.; Geological Society of London Special Publication: London, UK, 2008; Volume 293, pp. 35–55.
69. Ishimaru, S.; Arai, S. Peculiar Mg–Ca–Si metasomatism along a shear zone within the mantle wedge: Inference from fine-grained xenoliths from Avacha volcano, Kamchatka. *Contrib. Mineral. Petrol.* **2011**, *161*, 703–720. [[CrossRef](#)]
70. Latypov, R.; Costin, G.; Chistyakova, S.; Hunt, E.J.; Mukherjee, R.; Naldrett, T. Platinum-bearing chromite layers are caused by pressure reduction during magma ascent. *Nat. Commun.* **2018**, *9*, 462. [[CrossRef](#)] [[PubMed](#)]
71. Huang, J.; Hao, J.; Huang, F.; Sverjensky, D.A. Mobility of chromium in high temperature crustal and upper mantle fluids. *Geochem. Persp. Lett.* **2019**, *12*, 1–6. [[CrossRef](#)]

